

# 1 Investigating termite nest 2 thermodynamics using a quick-look 3 method and the heat equation

4  
5 Rémi Gouttefarde<sup>1\*</sup>, Richard Bon<sup>1</sup>, Vincent Fourcassié<sup>1</sup>, Patrick Arrufat<sup>1</sup>, Ives  
6 Haifig<sup>2</sup>, Christophe Baehr<sup>3</sup> & Christian Jost<sup>1</sup>  
7

8  
9 <sup>1</sup>Centre de Recherches sur la Cognition Animale (CRCA), Centre de Biologie Intégrative (CBI), Université  
10 de Toulouse : CNRS, UPS, UMR5169, France.

11 <sup>2</sup>Instituto de Ciências Agrárias, Universidade Federal de Uberlândia–UFU, Monte Carmelo-MG, Brasil

12 <sup>3</sup>Institut Mathématiques de Toulouse, Université de Toulouse : CNRS, UPS, Météo-France/CNRS,  
13 CNRM/UMR3589, France.

14  
15 \* Corresponding author

16 Email: [gouttefarde.remi@gmail.com](mailto:gouttefarde.remi@gmail.com)

## 17 Abstract

18 Termite mounds are often cited as an example of efficient thermoregulated structures.  
19 Nest thermal stability can be critical for insects that are particularly sensitive to heat and  
20 desiccation. Few studies have measured internal temperature of termite nests with  
21 respect to environmental parameters, especially in Neotropical species. In this study, we  
22 analyzed the thermal profiles of different parts of *Procornitermes araujoï* nests, a  
23 neotropical mound-building termite of the Brazilian *cerrado*. To read into our dataset we  
24 first used rasterization, a method that allows a quick-look assessment of time-series. Our  
25 results show that nest architecture efficiently buffers against environmental temperature  
26 fluctuations while at the same time maintaining a relatively high internal temperature in  
27 the core. This rather stable internal climate follows nevertheless the external temperature  
28 long-term averages. Using a novel numerical scheme, we further show that the heat  
29 transfer dynamics are well described by the classical heat equation, with an additional  
30 heat source whose origin is discussed.

## 31 Introduction

32 Nests are supposed to protect animals from hostile environmental conditions [1]. In  
33 social insects, nests can be considered as microclimate regulation devices (for gas exchange,  
34 temperature or humidity) and have intrigued researchers for decades [2–6]. They are also an  
35 inspiring source for human engineering applications [7–10]. Nest thermoregulation can be  
36 characterized as either active or passive [4]. Active thermoregulation is defined as mastered  
37 by insect behavior such as fanning behavior in bees [4] or the creation of an energy sink by  
38 bringing up underground water in termites [11]. On the other hand, passive  
39 thermoregulation relies on mechanisms such as nest site selection [4,12] or nest  
40 architecture [6]. An outstanding example of passive thermoregulation is the ventilation  
41 system developed by some ant and termite species to increase the ventilation of their  
42 underground chambers [7,13–17].

43 Nest temperature is highly influenced by external periodic forcing. Even if the nest  
44 structure generally permits a good regulation of the internal microclimate, nest  
45 temperatures often follow short term (daily) and long term (weekly, annual) environmental  
46 fluctuations [7,18]. In mound-building species, like the African termite *Trinervitermes sp.*, the  
47 temperature fluctuations are more important in the upper part of the mound than inside the  
48 core [18,19]. Here, we investigate temperature dynamics in the Neotropical termite  
49 *Procornitermes araujoi* Emerson (1952) [20]. This species is endemic to the Brazilian *cerrado*  
50 (savanna). Its colonies inhabit nests that are characterized by medium-sized mounds usually  
51 rising less than 1m above ground (**Fig 1a**). The internal architecture is relatively simple with  
52 an homogeneous foam-like structure (**Fig 1a**) [21,22] also found in *Trinervitermes sp* or even  
53 in ant species like the black-garden ant *Lasius niger* [23]. It lacks the complex ventilation  
54 systems found in fungus-growing termites [15,24] or in leaf-cutting ants [14]. It is thus a  
55 convenient species to study nest thermoregulation in simple architectures with lower  
56 metabolic activity compared to fungus growing species.

57  
58 **Fig 1. Experimental setup.** (a) Sagittal section of a *P. araujoi* nest showing the foam-like structure and the  
59 underground extension of the nest. Yellow or black squares are 5 x 5 cm. (b) *P. araujoi* nest with the  
60 monitoring wires. (c) Probe positions inside and around the nests and spatial parameters used in the heat  
61 equation.  $T_1$  = Temperature of the top;  $T_2$  = Temperature of the side;  $T_3$  = Temperature of the core;  $\Gamma_1$  = heat  
62 flux between the top and the side probes;  $\Gamma_2$  = heat flux between the side and the core probes;  $\Delta h$  = height

63 difference between the time derivative estimation  $\frac{\Delta T^n}{\Delta t}$  and the temperature heat flux gradient estimation  
64  $L_1^n$  (see text for equations).

65

66 In closed mounds like those built by *P. araujo*, nest material is likely to influence  
67 thermoregulation by affecting the microstructure of the walls and water retention, which  
68 are probably also crucial for gas exchange properties in such nests [16,25]. In *P. araujo*, the  
69 workers use soil, regurgitated soil, fecal material and saliva as construction material [21].  
70 Moreover, the mounds are often covered by a thin layer of loose soil and grass [20; personal  
71 observations] that could also have insulating properties [26].

72 In this study, we monitored nest temperature in different parts of *P. araujo* nests.  
73 Our aim was to characterize the buffering effect of the structure, that is the ability of the  
74 structure to regulate the internal temperature against external environmental fluctuations.  
75 Previous studies have shown that mounds are subject to daily and long term temperature  
76 fluctuations and that termites may contribute to this buffering effect [11,18]. To investigate  
77 nest thermoregulation, we propose a methodology that first identifies thermal patterns and  
78 then to quantify them using the heat equation.

79 From a technical point of view, detecting patterns in raw time series (as our data) can  
80 quickly become tricky [27–29]. Such technical difficulties can obfuscate the actual biological  
81 interpretation of the data. Here we first propose to use a quick-look method: rasterization  
82 [30–32]. This method consists in transforming 1D time series with a dominant periodic  
83 forcing (here daily fluctuation) into a 2D image that can be suitable for a quick visual  
84 inspection. In addition we transformed the data by using different thresholding and  
85 normalization schemes that allows to accentuate patterns in the rasterized images and thus  
86 helping to understand the overall dynamic patterns. This rasterization method first allows us  
87 to detect the nests' buffering efficiency at short (daily) and long (across days) scale. We then  
88 investigated the physics of the heat transfer dynamics inside the nests in the context of the  
89 heat equation. This equation predicts that (a) the mean temperature is independent of the  
90 monitored location in the nest, (b) the temperature amplitude decreases with increasing  
91 depth (distance to the top of the nest) *i.e.* shows mitigation, and (c) the phase shifts  
92 according to depth. A numerical scheme allows to fit the heat equation to the monitoring  
93 data. This fit provides two parameters to characterize the mound: the heat diffusion  
94 coefficient that quantifies the buffering effect (decreasing amplitude or mitigation), and a

95 constant that tells whether the living mound is globally a free system, an energy source or an  
 96 energy sink.

97

## 98 **Methods**

### 99 **Biological material and experimental field area**

100 Three nests of the termite *P. araujoii* were monitored during two weeks (04/11/2016-  
 101 18/11/2016) in a pasture located at the *Fazenda Capim Branco* (18°52'48''S, 48°20'27''W),  
 102 an area belonging to the Federal University of Uberlândia, Minas Gerais, Brazil (**S1 Fig**). The  
 103 circumference of each nest at different heights (corresponding to the levels where each  
 104 probe was inserted (**Figs 1b,c** and **Table S1**)) was measured to estimate the size of the nests.  
 105 The total volume of a nest was estimated as the sum of the volumes of each section. The  
 106 volume of the upper section (top of the nest) was calculated using the formula for the  
 107 volume of a cone ( $\pi \times R^2 \times h / 3$ , with  $h$  the cone height and  $R$  the radius at its base). For the  
 108 2 lower sections, the formula of a truncated cone ( $h \times \pi/3 \times (R_1^2 + R_2^2 + R_1 \times R_2)$ ) was used,  
 109 where  $R_1$  and  $R_2$  are the radiuses of the upper and lower discs respectively). The total  
 110 volumes were 0.34, 0.52 and 0.39 m<sup>3</sup> respectively for nests A, B and C (**Table 1**). Taxonomic  
 111 identification of the termite species was done using the soldier morphology following the  
 112 dichotomous identification keys of Constantino [33] for the genus and Canello [34,35] for  
 113 species identification.

114

115 **Table 1. Nest characteristics.**

Nest	Top of the nest		Top probe entrance		Side probe entrance		Core probe entrance		Basis		V
	H	C	H	C	H	C	H	C	H	C	
<b>A</b>	0.72	0	0.6	1.02	0.48	1.77	0.3	2.47	0	4.03	<b>0.34</b>
<b>B</b>	0.58	0	0.53	1.3	0.43	2.4	0.25	3.92	0	4.42	<b>0.52</b>
<b>C</b>	0.7	0	0.51	1.1	0.4	2.03	0.19	3.27	0	4.7	<b>0.39</b>

116

117 Height H (m) and circumference C (m) of the 3 nests at different levels corresponding to the probe entrance  
 118 points (see Fig 1c) with the resulting nest volume V.

119

## 120 **Nest monitoring**

121 Custom made devices (**S1 Text**) were used to measure the temperature every 10 min  
122 at five different positions, following Field & Duncan's protocol [18] (see **Figs 1b,c** and **Table**  
123 **S1** for details). Each probe was placed into a 2 cm diameter plastic tube. The tubes were  
124 sealed at one end with a mesh to prevent the termites from entering. The other end was  
125 sealed with silicone. A concrete drill of 2.5 cm diameter was used to dig the holes into the  
126 nest (from the east side) and the ground where the tubes were placed. For each nest, two  
127 probes were placed inside each tube at each position in case of failure of one. Probes were  
128 placed (1) at the top of the nest, 5 cm below the nest surface, (2) on the side, at a horizontal  
129 distance of 20 cm from the surface, (3) inside the core of the nest (40 cm depth with an  
130 angle of 45° compared to the horizontal), in the soil next to the nest (4) at 5 cm depth and  
131 (5) at 20 cm depth, (6) at 1 m distance from the nest at 20 cm depth. When all the probes  
132 were installed, the data-loggers were started. The probes placed at the same location gave  
133 quasi identical data (**Table S1**). Therefore, only one of the two probes was used for the  
134 analysis.

135 Environmental parameters (air temperature, solar radiation, precipitations and  
136 relative humidity) were monitored in the meteorological station of the *Fazenda Capim*  
137 *Branco* situated approximately at 500m from the experimental field area.

138

## 139 **Data visualization: the rasterization method**

140 Rasterization consists in transforming 1D time-series (see different examples of  
141 theoretical signals in **Fig 2a**) data into a 2D image by plotting the principal period (*e.g.* day,  
142 year, lunar month) on the y-axis, and subsequent periods on the x-axis; the actual signal is  
143 encoded in colors to obtain a heatmap like image (**Fig 2b**). Converting a time-series into a  
144 2D image not only allows decomposing the signal, but also applies a smoothing effect  
145 that reduces the details and emphasizes the general patterns.

146 In the case of a weak amplitude of the signal, some patterns can be masked by the  
147 color scale (**Fig 2b**). To solve this issue, one can enhance the contrast by normalization  
148 of the signal, for example into the range of [-1,1] (see **S2 Text eq (S2)**) (**Fig 2c**). This  
149 allows comparing easily the temporal dynamics of signals that have different amplitudes  
150 (**Fig 2a** and **2c**).

151 Another way to enhance contrast and facilitate pattern identification in  
152 rasterized images is to use hard thresholding (**Fig 2d**): it replaces each original value by  
153 one of two colors (binary data) according to a reference value used as a threshold. This  
154 allows to visualize the sign of the anomaly (that is defined as the departure of the value of  
155 a series from a reference value).

156 Finally, the dynamics of the time-series can be visualized by plotting the differences  
157 between subsequent values in the series (increments). These increments can also be  
158 normalized to increase contrast and facilitate pattern identification (**Fig 2e**).

159 All the plots were done with R 3.2.3 [36] (the dataset and an exemple of the script used to  
160 produce the figures are available online (<http://doi.org/10.5281/zenodo.822263>))

161

162 **Fig 2. Illustration of the rasterization method.** (a) “classical” 1D time-series for different kinds of theoretical  
163 signals sampled hourly. The horizontal color bar under the plots represents the encoding of the signal’s value in  
164 a color scale. Rasterized images of (b) the raw data of the 1D time series, (c) of the normalized data of the 1D  
165 time series, (d) of the sign of the departures from a reference value (anomaly), here the mean (values higher  
166 than the mean are plotted in magenta and those lower than the mean in blue), (e) of the normalized hourly  
167 increments.

168

## 169 **Dynamical characterization using the heat equation**

170 Here we investigate whether the spatio-temporal temperature evolution in the  
171 mound can be explained by a simple physical equation such as the heat equation. Using  
172 the *in-situ* temperature measurements, a numerical scheme of the heat equation is  
173 established in order to check whether this equation is able to predict the temperature  
174 inside the nest. This heat equation links linearly the temperature time derivative with  
175 the gradient of the heat fluxes. Both terms can be estimated from nest monitoring data if  
176 there are at least 3 probes.

177

## 178 **Mathematical background**

179 The heat transfer equation describes the propagation of heat inside a domain. In  
180 the context of a termite nest heated by the sun, the heat transfer follows the sunray line.  
181 We assume that the heat propagation is done along the vertical axis and therefore that  
182 the domain is one-dimensional and semi-bounded. The equation describes the time  
183 dynamics of the temperature, represented by the time derivative of the temperature

184 subject to the spatial variation of the vertical heat fluxes with a proportionality  
185 coefficient called the diffusivity coefficient.

186

187 The heat transfer is thus the partial differential equation

$$188 \quad \frac{\partial T}{\partial t} = D \frac{\partial^2 T}{\partial z^2}$$

189 that may be also written as

$$190 \quad \frac{\partial T}{\partial t} = \frac{\partial}{\partial z} \left( D \frac{\partial T}{\partial z} \right) = \frac{\partial}{\partial z} (D \gamma)$$

191 where  $T$  is the temperature (K) as a function of time  $t$  and depth  $z$ ,  $T = T(t, z)$ , and  $\gamma =$   
192  $\frac{\partial T}{\partial z} (K m^{-1})$  is the vertical heat flux. The boundary conditions of the semi-open domain  
193 are given by the surface temperature  $T_0 = T(t, 0)$ . The heat transfer coefficient  $D$  is a  
194 characteristic of the medium. In the present form of the heat equation, the medium is  
195 supposed to be homogeneous and  $D (m^2 s^{-1})$  is a constant.

196 The proportionality between the temperature time derivative  $\frac{\partial T}{\partial t}$  and the heat flux  
197 gradient  $\frac{\partial^2 T}{\partial z^2} (K m^{-2})$  describes the flow of heat. It is well known that the solution of  
198 this equation is a diffusion process. In the case of a sinusoidal surface temperature, an  
199 analytical solution of the heat equation is known. We consider that  $T_0(t) = T(t, 0) =$   
200  $A \sin(\omega t) + T_m$  where  $\omega$  is the pulsation in  $rad s^{-1}$ ,  $A$  is the amplitude of the sinusoidal  
201 function and  $T_m$  is the mean temperature. Then the analytical solution is:

$$202 \quad T(t, z) = T_m + A e^{-\sqrt{\frac{\omega}{2D}}z} \sin\left(\omega t - \sqrt{\frac{\omega}{2D}}z\right)$$

203 The solution of the above equation may be seen as the mean temperature, with an  
204 amplitude mitigation function relative to the depth and a phase difference in the sine  
205 function given by the depth. It is easy to transform the phase difference into a time lag.  
206 Indeed,

$$207 \quad \sin\left(\omega t - \sqrt{\frac{\omega}{2D}}z\right) = \sin\left(\omega \left(t - \frac{z}{\sqrt{2D\omega}}\right)\right)$$

208 Therefore, the mathematical solution of the 1D heat transfer equation in the case of a  
209 sinusoidal forcing contains the two characteristics seen below in the nest temperature  
210 measurements: a time lag and mitigation according to the depth  $z$ .

211

212 The heat transfer equation written previously corresponds to a free system. In the case  
213 of a non-autonomous system, with an energy well or forcing (such as heat absorption by  
214 water brought in by the termites or metabolic heat), the heat transfer equation is  
215 modified by an additive term,

$$216 \quad \frac{\partial T}{\partial t} = D \frac{\partial^2 T}{\partial z^2} + Q$$

217 The additive energy  $Q$  is a negative term in case of a loss of energy, that is an energy  
218 sink, and non-negative for an input of energy, that is a positive forcing.

219

## 220 Numerical approach

221 In order to link the heat equation to our temperature measurements at few  
222 discrete spots in the nest, it is necessary to discretize the partial differential equation.

223 This discretization has to take into account the time characteristic of the cycles  
224 according to the time step of the data. It also has to take into account the heat  
225 propagation inside the soil. The flux transfer and the heat propagation in the soil are  
226 slow processes compared to external temperature forcing. Therefore, before the  
227 computation of the time and spatial derivatives, the fast variations are filtered from the  
228 temperature measurements by using a Fourier low-pass filter. Since the mean diffusivity  
229 coefficient and the mean additive forcing are of interest, the frequency of this low-pass  
230 filter corresponds to the diurnal cycle of 24 hours.

231 The time derivative is directly estimated by the first order difference:  $\frac{\partial T}{\partial t} \sim \frac{\Delta T^n}{\Delta t}$  where  
232  $\Delta t$  is the data time step, and  $\Delta T^n$  is the difference  $\Delta T^n = T^n - T^{n-1}$  ( $T^n$  is the  
233 temperature at the time  $t^n = n\Delta t$ ). This temperature derivative series is estimated  
234 using the side probe  $T_2$ .

235 The vertical temperature Laplacian at a given depth,  $\Delta T$  is the temperature  
236 second derivative. This term is computed by two vertical derivatives. If  $T_j^n$  is the  
237 temperature for the time  $t^n = n\Delta t$  at the  $j$ -th depth, the heat flux  $\gamma = \frac{\partial T}{\partial z}$  is estimated by

238  $\frac{T_{j+1}^n - T_j^n}{\Delta z_{j+1,j}} = \Gamma_j^n$  where  $\Delta z_{j+1,j}$  is the distance between the  $(j+1)$ -th and the  $j$ -th probes,  $j =$

239 1 or 2. This flux is supposed to be estimated at the depth  $\frac{z_{j+1} + z_j}{2}$ . Using the three  
240 different depths, of our temperature measurements possible to compute two fluxes, and  
241 the second derivative of the temperature, which is the gradient of the heat flux, is then



242 computed with the same method in order to get  $\frac{\Gamma_2^n - \Gamma_1^n}{\Delta\lambda} = L_1^n$  where  $\Delta\lambda = \frac{z_3 - z_1}{2}$ . This term  
243  $L_1^n$  is supposed to be estimated at the depth  $\frac{z_1 + 2z_2 + z_3}{4}$ .

244 The estimates  $L_1^n$  have to be corrected by a time shifting (associated to  $\Delta h$  in Fig  
245 1c) in order to be adjusted to the temperature increment. Indeed, the distances between  
246 the probes are quite large and the time lag is about one hundred minutes per 10 cm,  
247 whereas the time step is about 10 min. Therefore a time shifting of the Laplacian  
248 estimation  $L_1$  is necessary. Several methods are possible to assess this time shift  
249 (Fourier spectral shift, maximum of cross-correlation function, ...). Here we estimated it  
250 as the number of time steps that maximize the absolute value of the correlation between  
251 temperature derivative  $\frac{\Delta T^n}{\Delta t}$  and the heat flux gradient  $L_1^n$ .

252 Finally, a linear regression between the time derivative  $\frac{\Delta T^n}{\Delta t}$  and the temperature  
253 second derivative  $L_1^n$  is performed. This regression provides estimates of the mean  
254 diffusivity coefficient  $D$  and of the mean additive forcing  $Q$ . Such a standard linear  
255 regression provides also the standard errors of these parameters. However, time series  
256 data do not fulfill the independence property assumed in these methods (our  
257 temperature time series are highly auto-correlated, leading to underestimated standard  
258 errors due to this pseudo-replication). Methods to correct for the bias induced by  
259 pseudo-replication are beginning to appear in the statistical literature [37] but their  
260 usefulness in the case of time series data is still strongly debated. We therefore chose  
261 not to report any standard errors for  $D$  and  $Q$  in a given nest, but to compute them with  
262 the classical formula over the three values obtained for our three (independently)  
263 monitored nests.

## 264 Results

265 The mean, standard deviation and coefficients of variation for each probe are given in **Table**  
 266 **2**. The mean temperatures monitored at the different locations of the nest as well as in the  
 267 soil are almost identical. For both the mound and the soil, the standard deviations decrease  
 268 with depth  $z$ , leading to decreasing coefficients of variation. The temperature amplitudes are  
 269 indeed much higher at the top of the nest (temperature range [16;44] °C) compared to the  
 270 core (temperature range [24;28] °C; **Fig 3a, S2 Fig**). The same applies to the comparison of  
 271 the soil temperatures at 5 and 20 cm. Mound temperatures are on average higher than soil  
 272 and air temperatures (**Fig 3a**). Note that the air temperature and its amplitude are similar to  
 273 those of the soil temperatures at 5 cm. In addition, daily variations of air temperature are  
 274 intermediate between the top and the core of the nest.

275

276 **Table 2. Descriptives statistics.**

	Nest A		Nest B		Nest C	
	<i>Mn ± SD (°C)</i>	<i>CV</i>	<i>Mn ± SD (°C)</i>	<i>CV</i>	<i>Mn ± SD (°C)</i>	<i>CV</i>
<i>Top</i>	25.82 ± 6.26	0.24	24.39 ± 4.46	0.18	25.54 ± 5.24	0.20
<i>Side</i>	27.00 ± 2.68	0.10	26.63 ± 2.73	0.10	25.89 ± 3.13	0.12
<i>Core</i>	26.42 ± 0.85	0.03	25.79 ± 0.52	0.02	25.64 ± 0.78	0.03
<i>Soil 5cm</i>	23.78 ± 3.42	0.14	NA	NA	23.59 ± 2.43	0.10
<i>Soil 20cm</i>	23.96 ± 1.34	0.06	24.50 ± 1.04	0.04	23.79 ± 0.72	0.03
<i>Air (station)</i>	<i>Mn ± SD (°C)</i>	<i>CV</i>				
	22.69 ± 3.36	0.15				

277

278 Mean (Mn), standard deviation (SD) and coefficient of variation (CV) of the temperature recorded by each  
 279 probe for the 3 nests and for the air (meteorological station) during the 14 days. NA corresponds to the case  
 280 where both inserted probes failed.

281

282 **Fig 3. Rasterization raw data (transform 1D time-series into a 2D image).** (a) for the 3 nests and all the probe  
 283 positions and (b) for the environmental parameters (air temperature, solar radiation, precipitations and  
 284 relative humidity). White space indicates missing data.

285

## 286 Interpretation of the rasterized images

287 The rasterized images of the raw data (**Fig 3a**) show comparable patterns for probes  
 288 at the same location in the three nests. In addition to the decreasing amplitudes (mitigation)

289 with increasing depth in both the nest and the soil, data also show that maximum  
290 temperatures are attained later in the evening with increasing depth (Fig 3a). However, on  
291 these figures one can barely see a pattern in the core or soil at depth 20cm. A clear pattern  
292 appears in both cases in **Fig 4** where we normalized the data into the range [-1;1]; maximum  
293 temperatures were much delayed compared to air and nest top ones (around 4 pm),  
294 occurring at midnight in the core. One can also see that the highest temperatures and the  
295 daily variation are smaller in all probe locations on days 11 and 12. This can be explained by  
296 cooler air temperature, less intense solar radiation and higher precipitations (with higher  
297 relative humidity, see **Fig 3b**) for these two days. This reveals that temperature of the nest  
298 follows the long-term environmental fluctuations and is true even for the core temperature  
299 although more attenuated than at the most peripheral locations in the nest and in the soil.

300

301 **Fig 4. Normalized rasterized data.** Data illustrated in Fig 3 (raw data) were normalized to restrict the values  
302 into a range of [-1;1] (see equation S1).

303

304 **Fig 5** shows the differential sensitivity of the upper part of the mound (top and side)  
305 and of the nest core to environmental fluctuations as revealed by the sign of the global  
306 anomaly of the time-series. The dominant vertical pattern seen in the core indicates that this  
307 latter is mainly sensitive to larger-scale external temperature changes while the dominant  
308 horizontal pattern seen in the top and side of the mound are more sensitive to the diurnal  
309 variation of the temperature. The pattern of anomaly shown in the soil at 5 cm and 20 cm  
310 depth are respectively quite similar to the ones observed at the top and the side of the nest  
311 showing that it follows principally daily fluctuations. The pattern of the side and soil at 20 cm  
312 reveals an intermediate pattern between the core and the surface (top of the mound and  
313 soil at 5 cm). Indeed, this pattern reflects both short (daily) and long (across days) term  
314 fluctuations. The relative long term fluctuations of the top and the side of the nest as well as  
315 of the soil at 5 cm can be visualized through the sign of the anomalies using the hourly mean  
316 temperature as threshold value (**Fig 6**).

317

318 **Fig 5. Rasterized sign of the anomalies using the overall mean as the threshold.** The positive anomaly is  
319 indicated in magenta and the negative anomaly in blue.

320

321 **Fig 6. Rasterized sign of the anomaly using the hourly means over the two weeks of observation period as**  
322 **the reference thresholds.** The positive anomaly is indicated in magenta and the negative anomaly in blue.  
323

## 324 **Dynamical characterization**

### 325 **Visualizing the heating and cooling phases**

326  
327 To visualize the temporal dynamics of heating and cooling, we plotted the hourly  
328 mean raw temperature at the different locations for the three nests (**Fig 7a**). We excluded  
329 days 11 and 12 which were different from the other days (**Fig 3**). The normalization of this  
330 data reveals a temporal shift of the maximum and minimum temperatures as one goes  
331 deeper inside the nest or in the soil (**Fig 7b**). Remarkably the heating and cooling of the core  
332 follows an inverted temporal pattern when compared to the top of the nest. Nevertheless, it  
333 is not easy to perceive whether the duration of the heating or the cooling are the same. This  
334 is easier to assess on the rasterized image of the normalized temperature increments  
335 following **eq S1** (**Fig 8**). The heating phase is well identified by the dominant magenta  
336 coloring, while the cooling phase has dominant blue coloring. Whatever the location, the  
337 heating phase is shorter than the cooling phase. We also notice that these two phases  
338 tended to be less asymmetric the deeper the probe location. The alternating pattern of 0  
339 and of non-zero values in the least-varying core temperatures illustrates rather slow periods  
340 of heating and cooling (see **eq S1**). By contrast, the almost continuous color patterns at the  
341 top and the side of the nest indicate faster heating and cooling periods preceded or followed  
342 by a rather long period of stationary temperatures centered around midnight.

343

344 **Fig 7. Mean temperatures along a 24h period.** (a) Mean temperatures during the day after excluding days 11  
345 and 12. (b) Normalized curves (between [-1 ;1]) of the same mean temperatures.

346

347 **Fig 8. Rasterized increments of the raw data.** The amplitudes of the increments  $\Delta T^n$  are normalized to restrain  
348 the values into a range of [-1;1].

349

## 350 **Nest diffusivity coefficient**

351 **Fig 7. Estimation of the temperature time derivative ( $\frac{\partial T}{\partial t}$ ) and the flux spatial gradient ( $\frac{\partial y}{\partial z} = \frac{\partial^2 T}{\partial z^2}$ ) for nest A.** (a)  
352 time derivative as a function of the flux spatial gradient, with the best fitting line (red) to estimate the

353 diffusivity coefficient  $D$  and the energy source  $Q$ , (b) the time derivative and its linear prediction from the  
 354 spatial flux gradient as a function of time, (c) the residuals of the linear regression in (a) as a function of time.  
 355

356 **Table 3. Estimated diffusivity coefficients and forcing terms in the three nests.**

Nest	Diffusivity Coefficient $D \times 10^{-6} (\text{m}^2 \text{s}^{-1})$	Forcing term $Q \times 10^{-4} (\text{K}/\text{s})$	Adjusted $R^2$	$\Delta z^{2,1} (\text{m})$	$\Delta z^{3,2} (\text{m})$	Time shift (min)
A	0.27	0.41	0.94	0.12	0.39	80
B	0.35	1.22	0.88	0.10	0.39	90
C	0.80	0.40	0.88	0.11	0.42	170
mean±se	$0.47 \pm 0.16$	$0.68 \pm 0.27$				

357  
 358 The  $\Delta Z$  are the vertical distances between the probes and the time shift is the one used in the estimation of  
 359 the heat flux gradients  $L_1^n$   
 360

361 **Fig 9a** shows the relationship between the time derivative and the spatial flux derivative for  
 362 nest A; the data are organized along a flat ellipse, a linear regression thus makes sense. The  
 363 associated residual structure in **Fig 9c** confirms this conclusion. **Fig 9b** shows the time  
 364 derivative and its linear prediction from the spatial flux gradient: there is a good agreement  
 365 between the two series. The two other nests give quite similar plots.

366 The estimated parameters of the heat equation for the three nests are summarized in **Table**  
 367 **3**. Nests A and B have coefficients of the same order, with  $D \sim 0.31 - 0.51 \cdot 10^{-6} \text{m}^2 \text{s}^{-1}$ . Nest  
 368 C's diffusivity coefficient is doubled. The mean additive forcings  $Q$  are all positive and in the  
 369 range  $0.37 - 1.24 \cdot 10^{-4} \text{K s}^{-1}$ . The time lag is about 70-80 minutes for nests A and B, and  
 370 about 170 minutes for nest C. In conclusion, nest C seems to have a behavior different than  
 371 the two other nests.

## 372 Discussion

373 Termite mounds are historically cited as an example of thermoregulated  
 374 constructions [6]. Nevertheless, recent studies rather suggest that there is no active  
 375 thermoregulation in these structures, even in the complex mounds of the fungus growing  
 376 termite *Macrotermes michaelseni* [7]. Here, we measured temperature at different positions  
 377 in the nest of the Neotropical mound-building termite *P. araujoii*. We aimed to characterize  
 378 the dynamics of heat propagation and to investigate how the structure reacts to external

379 forcing. We first used rasterized images to visualize our data and to decompose the effects  
380 of the diurnal and the large scale temporal forcing on temperature in the different parts of  
381 the nest. The results show that nest temperatures are strongly correlated with external  
382 forcing (solar radiation, rain), an argument for the weakness or absence of active  
383 thermoregulation. Nevertheless, even these simple homogeneous foam-like architectures  
384 show interesting thermal properties. Our results show indeed that the temperature pattern  
385 of the mound core differs from the top and the side of the mound as well as from the soil  
386 (both at 5 cm and 20 cm depth). On the one hand the core temperatures are very stable on a  
387 daily scale, while there are more important temperature fluctuations for the rest of the  
388 mound and the soil (**Fig 3** and **Table 2**). They are also higher than in the soil, thus providing a  
389 warm and very stable environment for the termites. On the other hand, it is also clear that  
390 the core, like the other parts of the mound and the soil, undergoes long term variations as  
391 the pattern observed for the core in Figs 4 and 5 corresponds to the one observed for the  
392 meteorological data (**Fig 3b**). These results confirm the findings on the mounds of the  
393 African termite *Trinervitermes sp.* which builds nests with similar architecture [18,19]. In  
394 particular, the increased core temperature has been found during the whole year [18] and is  
395 thus not only a simple consequence of monitoring temperature during the summer as we  
396 did.

397 From a functional point of view, the stable and warm temperature of the nest core  
398 might have significant effects on individual and colony development. Termites are  
399 hemimetabolous insects that undergo successive molting events during their life. In  
400 particular, during the post-embryonic development of termitid species, such as *P. araujoi*,  
401 the larvae follow one of either the apterous line, from which workers and soldiers originate,  
402 or the imaginal line from which alates originate [38]. Stable temperature may accelerate the  
403 rate of juvenile development [39], as it is the case in the nursery chambers of the nests of  
404 Macrotermitinae species (reviewed in [2]). Temperature can also influence caste  
405 composition [40,41]. Temperature variations may thus have a strong impact on the colony  
406 homeostasis which is based on the division of labor between the different categories of  
407 individuals which perform different behavioral activities [42].

408 In contrast to nests of *T. trinervoides* [18] our species' nests extend below ground. A  
409 comparison between the core and soil temperature dynamics is therefore relevant. Though  
410 the patterns observed for the core are relatively similar to the ones for the soil at 20 cm

411 depth, there are strong differences between the two concerning the dynamics of cooling and  
412 heating (**Figs 7 and 8**). The heating phase occurs later in the core compared to the soil. This  
413 could be explained by the fact that it takes much more time for the heat to propagate from  
414 the top of the mound which lies at 60-70 cm above the soil, than it takes to propagate from  
415 the soil surface to the 20 cm depth probe. Moreover, in the increments plot (**Fig 8**) one can  
416 see that the spacing between the discrete lines during the heating phase is tighter in the soil  
417 than in the nest's core, showing clearly that the latter has more efficient buffering properties  
418 against external forcing. Compared to the soil, the mound core therefore provides a more  
419 stable (and warmer) environment for the termites. Note that temperature increments are  
420 negatively correlated with spatial temperature variation between probes (**Figs 4 and 8**),  
421 indicating that it is relevant to analyze nest temperature dynamics in the context of the  
422 general heat equation. In fact, our analysis suggests that the heat equation explains well the  
423 diffusion of heat inside the mound structure. Our estimation of the heat diffusivity  
424 coefficients are similar to those of soils of similar composition [43]. The higher diffusivity  
425 coefficient and time shift of nest C (Table 3) could be natural variation in our small sample or  
426 the particular position of this nest at the base of a steep slope in the field (Fig S1). To further  
427 investigate the effect of architecture or topographic environment on heat diffusion the  
428 mound and soil diffusivity should be compared in a paired design (at least 3 probes in both  
429 the nest and the adjacent soil) with more monitored nests. Bristow *et al* [11] had already  
430 used the heat equation to detect an energy sink in the mound-building termite  
431 *Tumulitermes pastinator*. Our numerical scheme goes significantly further in terms of model  
432 validation, precision and parameter estimation. The results obtained in *T. trinervoides* [18]  
433 suggest that mound temperature is increased in the presence of termites. However, simple  
434 metabolic heat has been ruled out in the case of *M. michaelsoni* [7] which, as a fungus  
435 growing termite, produces much more metabolic heat than *P. araujoii*. An increase in  
436 temperature could be induced more actively by the termites [44] or by the mound design  
437 itself. Whatever the origin of this additional source of energy, our methodology permits to  
438 precisely quantify its value.

439 We think that the methodology we proposed here could be useful for future studies  
440 aiming to understand the mechanisms underlying termite nest thermoregulation. From a  
441 physical and evolutionary point of view a comparative approach between sympatric species  
442 that only differ by their mound architecture would be particularly interesting. In the case of

443 *P. araujoi* we suggest to compare to *Cornitermes cumulans* (whose individuals are close in  
444 size but whose mound architecture is much more elaborated with solid outer walls and soft  
445 organic inner space [45,46]) or to *Cornitermes bequaerti* (whose mounds are not closed but  
446 have outside openings for ventilation [46,47]).

447 To conclude, rasterization allowed a quick assessment of temperature monitoring  
448 data, suggesting the heat equation could govern nest temperature dynamics. The  
449 parameters of the heat equation were estimated from the monitoring data in order to  
450 characterize the overall nest temperature dynamics. To our knowledge this is the first study  
451 that develops a numerical scheme to link the heat equation to mound temperature  
452 dynamics and thus validates its pertinence for the studied system.

## 453 **Acknowledgements**

454 We would like to thank Tiago F. Carrijo from the Universidade Federal do ABC for his help  
455 with termite taxonomy and field work and Felipe Magalhães from the Universidade Federal  
456 de Uberlândia for providing the experimental field area. RG and VF received a financial  
457 support from the Université Toulouse 3 – Paul Sabatier for their field trip in Brazil.

## 458 **Author contributions**

459 RG, RB, VF and CJ designed the experiments. RG, VF and IH did the field work. IH provided  
460 field support. PA designed and constructed the data logger. RG, CB and CJ did the data  
461 analyzes and wrote the manuscript. All authors discussed and commented on the  
462 manuscript.

## 463 **Competing financial interests**

464 There are no competing financial interests involved in this paper.

## 465 **References**

- 466 1. Hansell M. Built by animals: the natural history of animal architecture [Internet].  
467 Oxford Uni. Oxford University Press; 2007. doi:10.1086/592657
- 468 2. Noirot C, Darlington JPEC. Termite Nests: Architecture, Regulation, and Defense.  
469 Termit Evol Soc Symbiosis Ecol. 2000; 121–139.
- 470 3. Darlington JPEC, Zimmerman PR, Greenberg J, Westberg C, Bakwin P. Production



- 471 of metabolic gases by nests of the termite *Macrotermes jeanneli* in Kenya. *J Trop*  
472 *Ecol.* 1997;13: 491. doi:10.1017/S0266467400010671
- 473 4. Jones JC, Oldroyd BP. Nest Thermoregulation in Social Insects. *Adv In Insect Phys.*  
474 2006;33: 153–191. doi:10.1016/S0065-2806(06)33003-2
- 475 5. Korb J. Termite mound architecture, from function to construction. In: Bignell DE,  
476 Roisin Y, Lo N, editors. *Biology of Termites: A Modern Synthesis*. Springer P.  
477 Heidelberg: Springer Press; 2011. pp. 349–373.
- 478 6. Lüscher M. Air-conditioned termite nests. *Sci Am.* 1961;205: 138–145.  
479 doi:10.1038/scientificamerican0761-138
- 480 7. Turner JS, Soar RC. Beyond biomimicry : What termites can tell us about realizing  
481 the living building . First International Conference on Industrialized, Intelligent  
482 Construction (I3CON). 2008. pp. 14–16.
- 483 8. Ball P. Bright lights, bug city. *New Sci.* 2010;2748: 35–37.
- 484 9. Holbrook CT, Clark RM, Moore D, Overson RP, Penick CA, Smith AA. Social insects  
485 inspire human design. *Biol Lett.* 2010;6: 431–433. doi:10.1098/rsbl.2010.0270
- 486 10. Werfel J, Petersen K, Nagpal R. Designing Collective Behavior in a Termite-  
487 Inspired Robot Construction Team. *Science* (80- ). 2014;343: 754–758.  
488 doi:10.1103/PhysRevE.89.012113
- 489 11. Bristow KL, Holt JA, Cloud S. Can termites create local energy sinks to regulate  
490 mound temperature? *J Therm Biol.* 1987;12: 19–21.
- 491 12. Chen Y, Hansen LD, Brown JJ. Nesting sites of the carpenter ant, *Camponotus*  
492 *vicinus* (Mayr) (Hymenoptera: Formicidae) in northern Idaho. *Environ Entomol.*  
493 2002;31: 1037–1042. doi:10.1603/0046-225X-31.6.1037
- 494 13. Kleineidam CJ, Roces F. Carbon dioxide concentrations and nest ventilation in  
495 nests of the leaf-cutting ant *Atta vollenweideri*. *Insectes Soc.* 2000;47: 241–248.  
496 doi:10.1007/PL00001710
- 497 14. Kleineidam CJ, Ernst R, Roces F. Wind-induced ventilation of the giant nests of the  
498 leaf-cutting ant *Atta vollenweideri*. *Naturwissenschaften.* 2001;88: 301–305.  
499 doi:10.1007/s001140100235
- 500 15. Turner SJ. Ventilation and thermal constancy of a colony of a southern African  
501 termite (*Odontotermes transvaalensis*: Macrotermitinae). *J Arid Environ.* 1994;28:  
502 231–248.
- 503 16. King H, Ocko S, Mahadevan L. Termite mounds harness diurnal temperature

- 504 oscillations for ventilation. Proc Natl Acad Sci U S A. 2015;112: 11589–11593.  
505 doi:10.1073/pnas.1423242112
- 506 17. Korb J. Thermoregulation and ventilation of termite mounds.  
507 Naturwissenschaften. 2003;90: 212–219. doi:10.1007/s00114-002-0401-4
- 508 18. Field MA, Duncan FD. Does thermoregulation occur in the mounds of the  
509 harvester termites, *Trinervitermes trinervoides* (Sjöstedt) (Isoptera :  
510 Termitidae)? African Entomol. 2013;21: 45–57.
- 511 19. Josens G. Variations thermiques dans les nids de *Trinervitermes geminatus*  
512 Wasmann, en relation avec le milieu extérieur dans la savane de Lamto (Côte  
513 d’Ivoire). Insectes Soc. 1971;18: 1–14.
- 514 20. Emerson AE. The neotropical genera *Procornitermes* and *Cornitermes* (Isoptera,  
515 Termitidae). Am Museum Nat Hist. 1952;99: 475–540.
- 516 21. Coles de Negret HR, Redford KH. The biology of nine termite species (Isoptera:  
517 Termitidae) from the cerrado of central Brazil. Psyche (Stuttg). 1982;89: 81–106.
- 518 22. Fouquet D, Costa-Leonardo a. M, Fournier R, Blanco S, Jost C. Coordination of  
519 construction behavior in the termite *Procornitermes araujoi*: structure is a  
520 stronger stimulus than volatile marking. Insectes Soc. 2014;61: 253–264.  
521 doi:10.1007/s00040-014-0350-x
- 522 23. Khuong A, Gautrais J, Perna A, Sbaï C, Combe M, Kuntz P, et al. Stigmergic  
523 construction and topochemical information shape ant nest architecture. Proc Natl  
524 Acad Sci U S A. 2016;113: 1303–1308. doi:10.1073/pnas.1509829113
- 525 24. Turner SJ. On the mound of *Macrotermes michaelsoni* as an organ of respiratory  
526 gas exchange. Physiol Biochem Zool. 2001;74: 798–822. doi:10.1086/323990
- 527 25. Cosarinsky MI. The nest growth of the Neotropical mound-building termite ,  
528 *Cornitermes cumulans* : A micromorphological analysis. J insect Sci. 2011;11: 1–  
529 14.
- 530 26. Bollazzi M, Roces F. The thermoregulatory function of thatched nests in the South  
531 American grass-cutting ant, *Acromyrmex heyeri*. J Insect Sci. 2010;10: 137.  
532 doi:10.1673/031.010.13701
- 533 27. Platt TR, Denman KL. Spectral analysis in ecology. Annu Rev Ecol Syst. 1975;6:  
534 189–210.
- 535 28. Daubechies I. Ten Lectures on Wavelets. Philadelphia: PA :Society for Industrial  
536 and Applied Mathematics; 1992.

- 537 doi:<http://dx.doi.org/10.1137/1.9781611970104>
- 538 29. Cazelles B, Chavez M, Berteaux D, Ménard F, Vik JO, Jenouvrier S, et al. Wavelet  
539 analysis of ecological time series. *Oecologia*. 2008;156: 287–304.  
540 doi:10.1007/s00442-008-0993-2
- 541 30. Koehler RB. Raster based analysis and visualization of hydrologic time series  
542 [Internet]. University of Arizona. 2004. Available:  
543 [http://arizona.openrepository.com/arizona/bitstream/10150/280516/1/azu\\_td\\_3131610\\_sip1\\_m.pdf](http://arizona.openrepository.com/arizona/bitstream/10150/280516/1/azu_td_3131610_sip1_m.pdf).  
544
- 545 31. Koehler RB. Innovative Ways to Visualize and Analyze Environmental Time-Series  
546 Data [Internet]. 2014. Available:  
547 [https://www.lib.noaa.gov/about/news/Koehler\\_aug202014.pdf](https://www.lib.noaa.gov/about/news/Koehler_aug202014.pdf)
- 548 32. de Pessôa JA. Pluviometric ID: Precipitation characteristics at a glance. *Atmos Sci*  
549 *Lett*. 2014;15: 288–291. doi:10.1002/asl2.501
- 550 33. Constantino R. Chave Ilustrada Para Identificação Dos Gêneros De Cupins (Insecta:  
551 Isoptera) Que Ocorrem No Brasil. *Pap Avulsos Zool*. 1999;40: 387–448.
- 552 34. Canello EM. Revisão de *Procornitermes Emerson* (Isoptera, Termitidae,  
553 *Nasutermitinae*). *Papéis Avulsos Zool (São Paulo)*. 1986;36: 189–236.
- 554 35. Canello EM, Rocha MM. Comparative morphology of the digestive tube in species  
555 of *Procornitermes Emerson* (Isoptera, Termitidae, *Syntermitinae*). *Mitteilungen*  
556 *aus dem Museum fur Naturkd Berlin - Dtsch Entomol Zeitschrift*. 2013;60: 147–  
557 153. doi:10.1002/mmnd.201300020
- 558 36. R Core Team. R: A language and environment for statistical computing. Vienna,  
559 Austria: R Foundation for Statistical Computing; 2015.
- 560 37. Davison AC, Hinkley D V. *Bootstrap Methods and their Application*.  
561 *Technometrics*. 1997;42: 216. doi:10.2307/1271471
- 562 38. Roisin Y. Diversity and evolution of caste patterns. In: Abe T, Bignell DE, Higashi  
563 M, editors. *Termites: Evolution, Sociality, Symbioses, Ecology*. Kluwer Aca.  
564 London: Kluwer Academic Publishers; 2000. pp. 95–119.
- 565 39. Mukerji D. Embryology of termites. In: Krishna K, Weesner FM, editors. *Biology of*  
566 *Termites*. New York A. New York: New York Academic Press; 1970. pp. 37–72.
- 567 40. Sattar A, Naeem M, Ul-Haq E. Impact of environmental factors on the population  
568 dynamics , density and foraging activities of *Odontotermes lokanandi* and  
569 *Microtermes obesi* in Islamabad. *Springerplus*. 2013;349: 1–7.

- 570 41. Scharf ME, Buckspan CE, Grzymala TL, Zhou X. Regulation of polyphenic caste  
571 differentiation in the termite *Reticulitermes flavipes* by interaction of intrinsic  
572 and extrinsic factors. *J Exp Biol.* 2007; 4390–4398. doi:10.1242/jeb.010876
- 573 42. Costa-Leonardo AM, Haifig I. Termite communication during different behavioral  
574 activities. In: Witzany G, editor. *Biocommunication of Animals*. Springer S.  
575 Springer Science+Business Media Dordrecht; 2014. pp. 161–190.
- 576 43. Márquez JMAM, Bohórquez MÁM, Melgar SG. Ground thermal diffusivity  
577 calculation by direct soil temperature measurement. application to very low  
578 enthalpy geothermal energy systems. *Sensors (Switzerland)*. 2016;16.  
579 doi:10.3390/s16030306
- 580 44. Korb J, Linsenmair KE. Thermoregulation of termite mounds: what role does  
581 ambient temperature and metabolism of the colony play? *Insectes Soc.* 2000;47:  
582 357–363. doi:10.1007/PL00001731
- 583 45. Grassé P-P. Sur le Nid Et La Biologie De *Cornitermes cumulans* (Kollar), Termites  
584 Brésilien. *Insectes Soc.* 1958;5: 189–199.
- 585 46. Ferreira de Barros MF. Os ninhos de *Cornitermes cumulans* (Kollar, 1832) e  
586 *Cornitermes bequaerti* (Emerson, 1952) (Isoptera: Termitidae): Estrutura,  
587 População e Animais Associados. UNESP Botucatu. 1994.
- 588 47. Fernandes PM, Czapak C, Veloso VRS. Cupins de montículo em pastagens: prejuízo  
589 real ou praga estética? In: Fontes LR, Berti Filho E, editors. *Cupins O desafio do*  
590 *conhecimento*. Piracicaba. Piracicaba: FEALQ; pp. 187–210.  
591  
592  
593

## 594 Supporting Information

595 **S1 Text. Data loggers.** Data loggers are designed to work autonomously for several weeks. They store  
596 temperature every ten minutes on an SD card (Secure Digital). The data logger has 3 main parts:

- 597 - 10 sensors measuring temperature (SHT25, Sensirion AG, Staefa ZH, Switzerland)
- 598 - Mass storage (2GB micro SD card, Transcend Information - Inc., Taipei, Taiwan)
- 599 - Microprocessor (PIC18F26K22, Microchip Technology, Chandler, Arizona, United States)

600 The processor coordinates the actions via an internal clock activated every ten minutes. It sequentially  
601 accesses each of the ten sensors, reads the temperature and stores these ten values in an internal RAM  
602 (Random Access Memory). Every 40 minutes, data in RAM are converted to ASCII (American Standard  
603 Code for Information Interchange) and then saved on the SD card in a standard CSV format (Comma-  
604 Separated Values). This implementation contributes to the long autonomy of the device. The data is coded  
605 on sixteen bits (maximum 65535 or five ASCII characters). The fourteen most significant bits represent  
606 the measured value and the two least significant bits contain status information that is not used here.  
607 These two bits must be set to zero for the calculation of temperature detailed below. Temperature  $T$  ( $S_T$  in  
608 binary format) is obtained through the transformation:

$$609 \quad T = -46.85 + 175.72 \left( \frac{S_T}{2^{16}} \right) \quad (S1)$$

610 According to the SHT25 datasheet, the accuracy tolerance of the sensor is +/- 0.2°C in the normal range of  
611 use. For further energy economy the resolution of the analogue-to-digital conversion was chosen on 11  
612 bits (faster reading times), which allows a resolution of approximately 0.08 °C (linearized values).

613

614 **S1 Table. Differences between homologous probes.**

615

	Probe	Mean diff (°C)	SD diff (°C)
<b>Nest A</b>	<i>Core</i>	-0.056	0.043
	<i>Side</i>	-0.056	0.043
	<i>Top</i>	-0.056	0.043
<b>Nest B</b>	<i>Core</i>	0.063	0.11
	<i>Side</i>	0.063	0.11
	<i>Top</i>	0.063	0.11
<b>Nest C</b>	<i>Core</i>	0.01	0.092
	<i>Side</i>	0.01	0.092
	<i>Top</i>	0.01	0.092

616

617 For all the nest positions, two probes were placed in the same tube. We calculated the mean and standard  
618 deviation of the differences for each of these pair of probes for the 3 nests.

619

620 **S2 Text. Data normalization.** The data presented in **Figs 1e, 1f** and **1i** were normalised using the  
621 following formula:

622 
$$xnorm_i = 2 * \left( \frac{x_i - x_{min}}{x_{max} - x_{min}} \right) - 1 \quad (S2)$$

623 After applying this transformation, the new data values  $xnorm_i$  are bound between -1 and 1.

624

625 **S1 Fig. Experimental field area.** The labels indicate the nest positions in the field. The line A/A' indicates  
626 a sagittal section of the field (inset) showing the slope and altitude difference between the nest C and the  
627 two other nests (A and B). Map data © 2017 Google, Imagery © 2017, CNES/Airbus, DigitalGlobe.

628

629 **S2 Fig. Raw time series data for the 3 nests.** The lines are the raw temperatures as a function of time for  
630 the different probe locations.

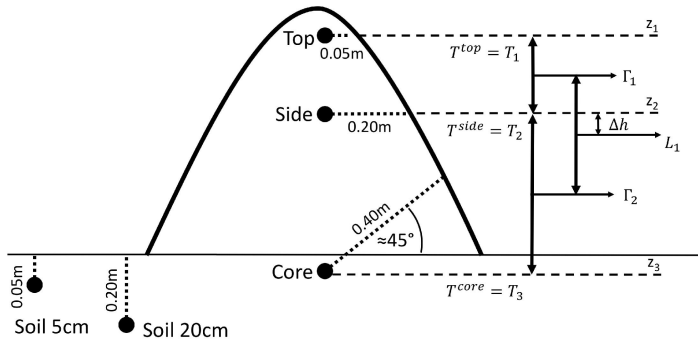
631

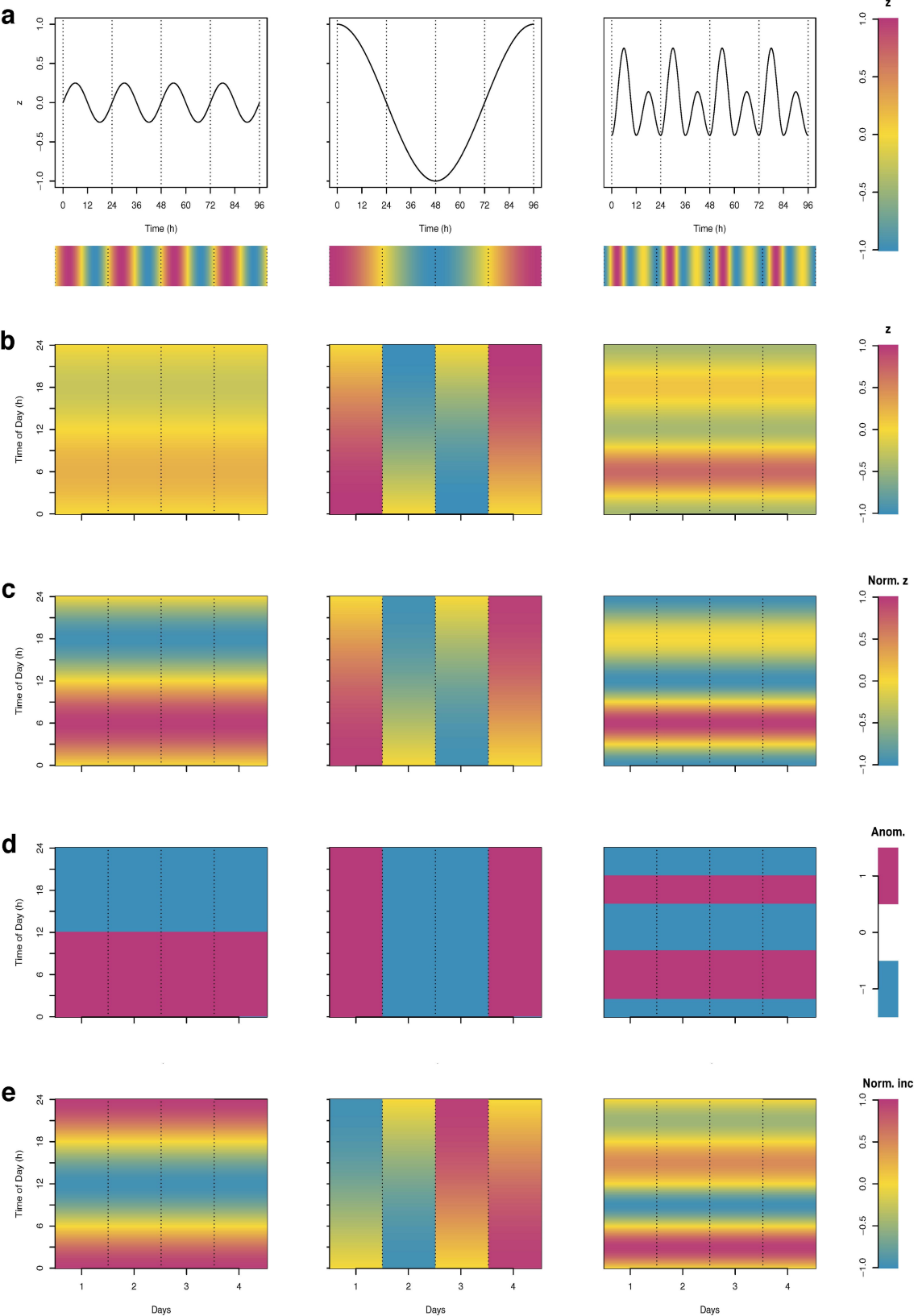
632

633

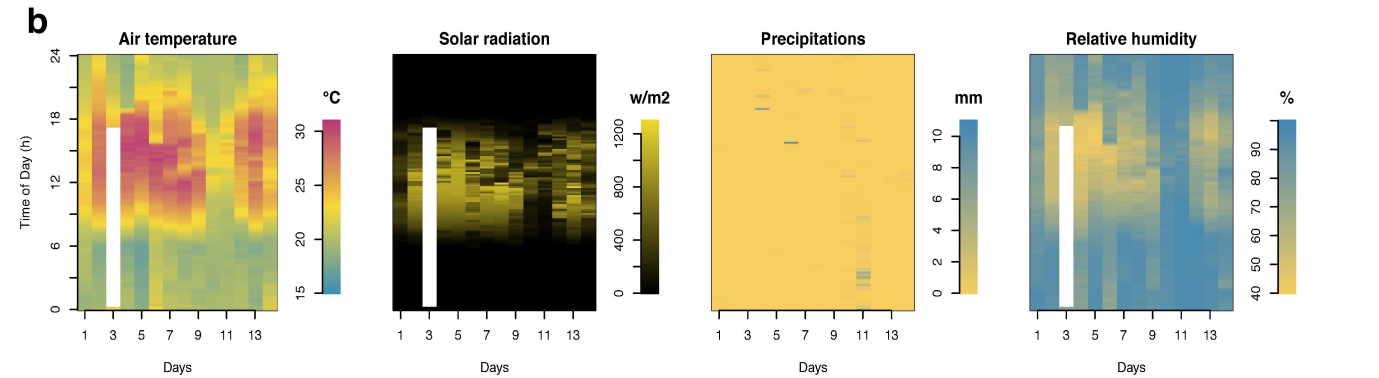
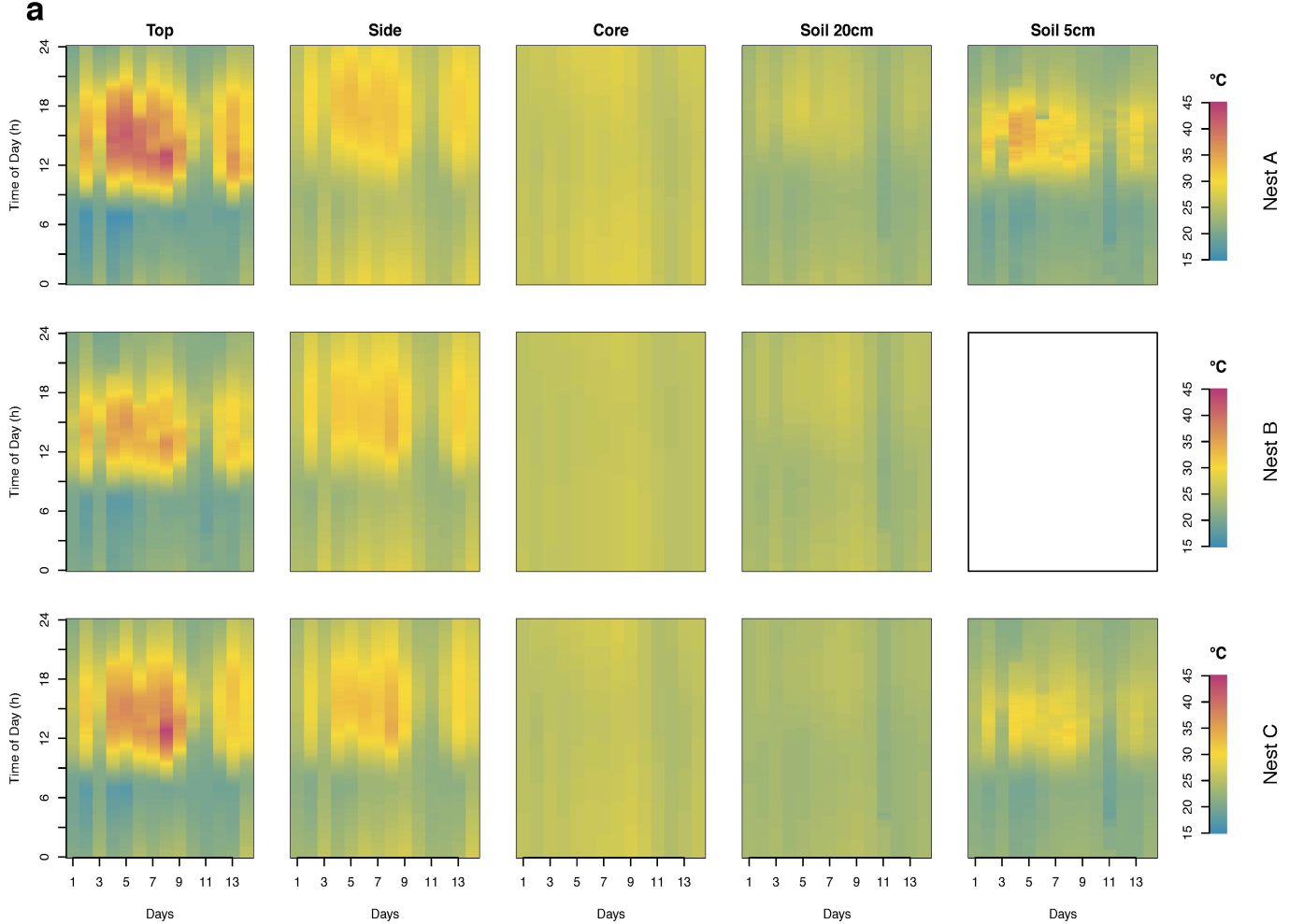
634

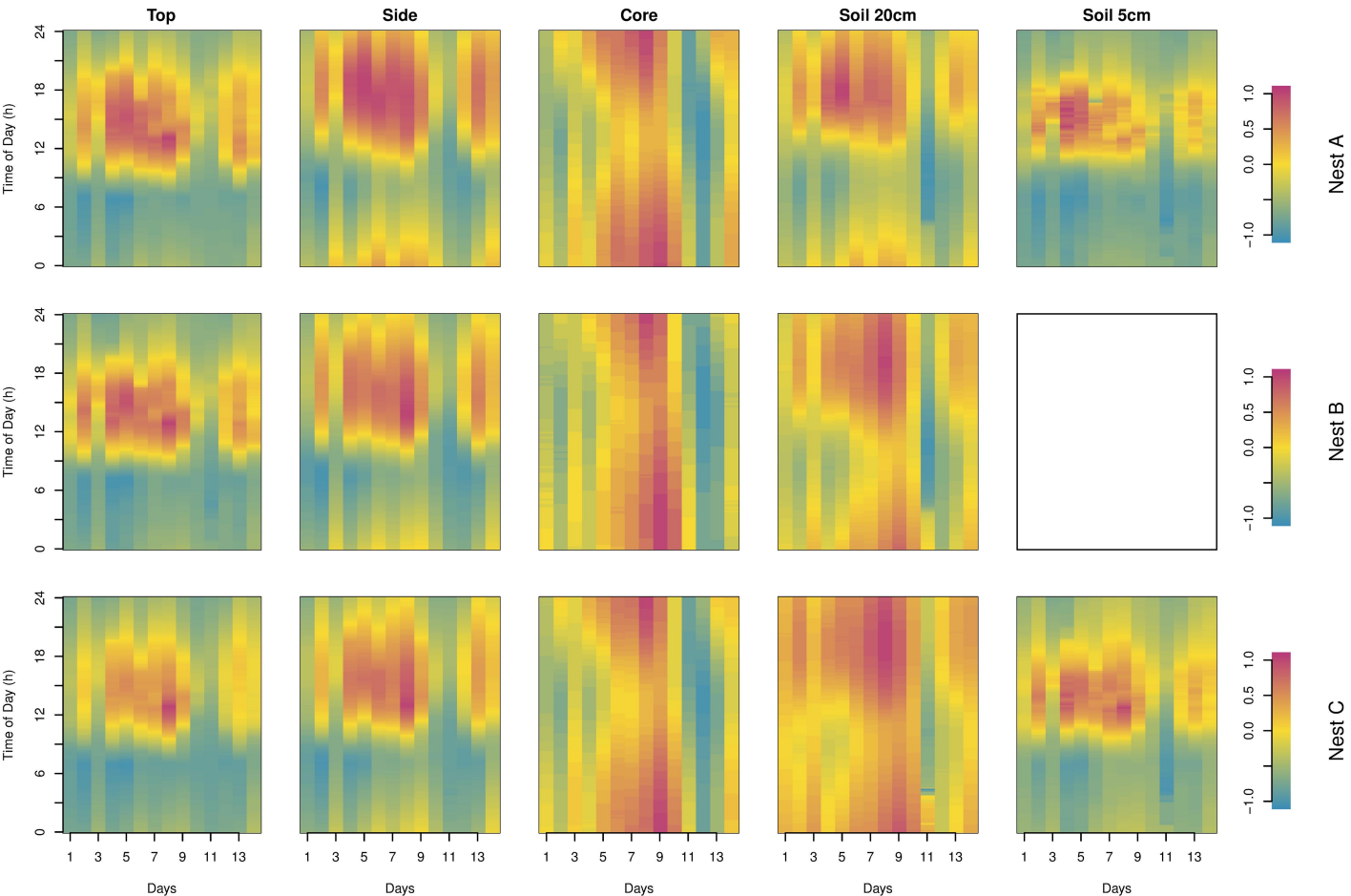
635

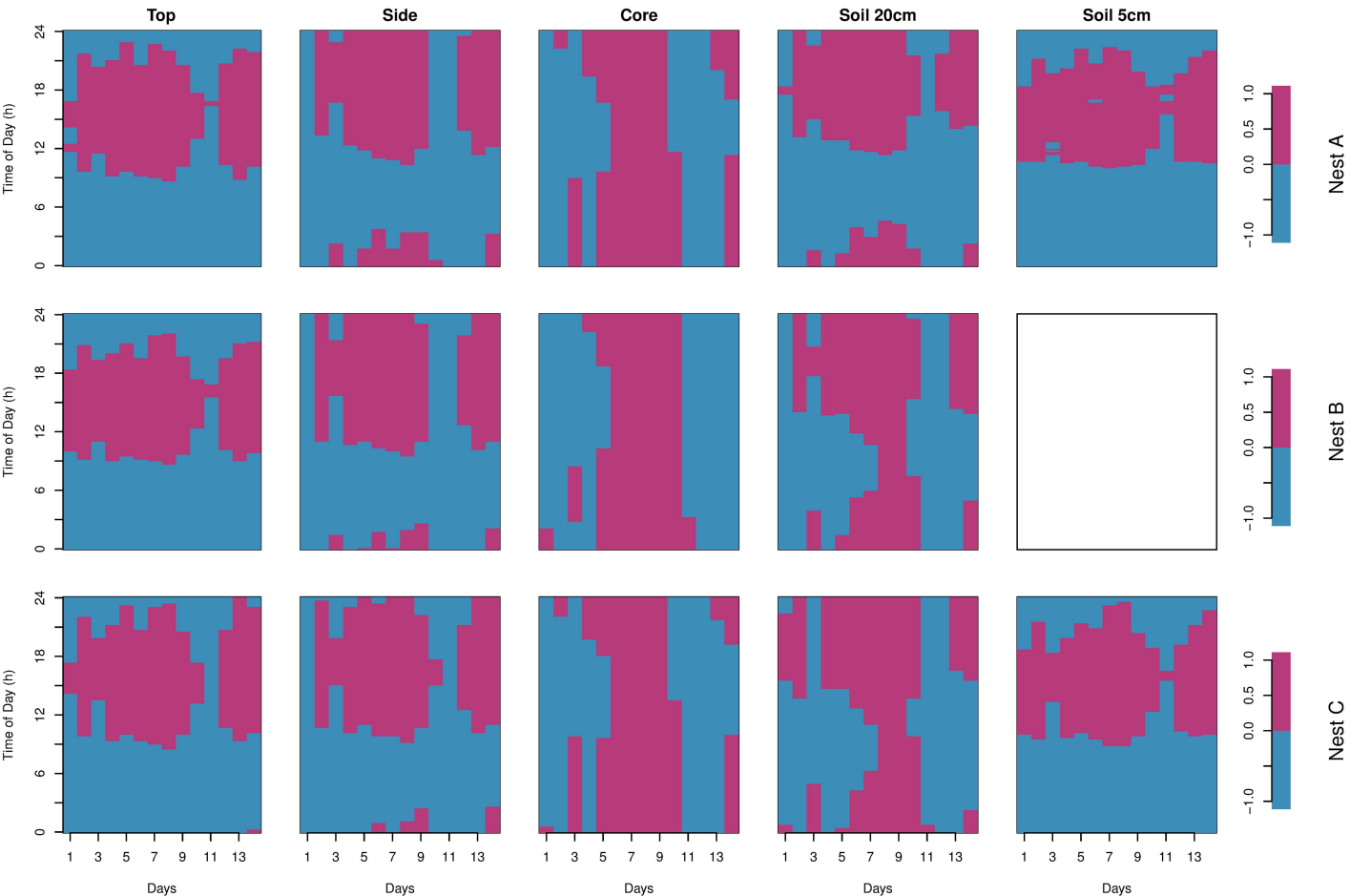
**a****b****c**

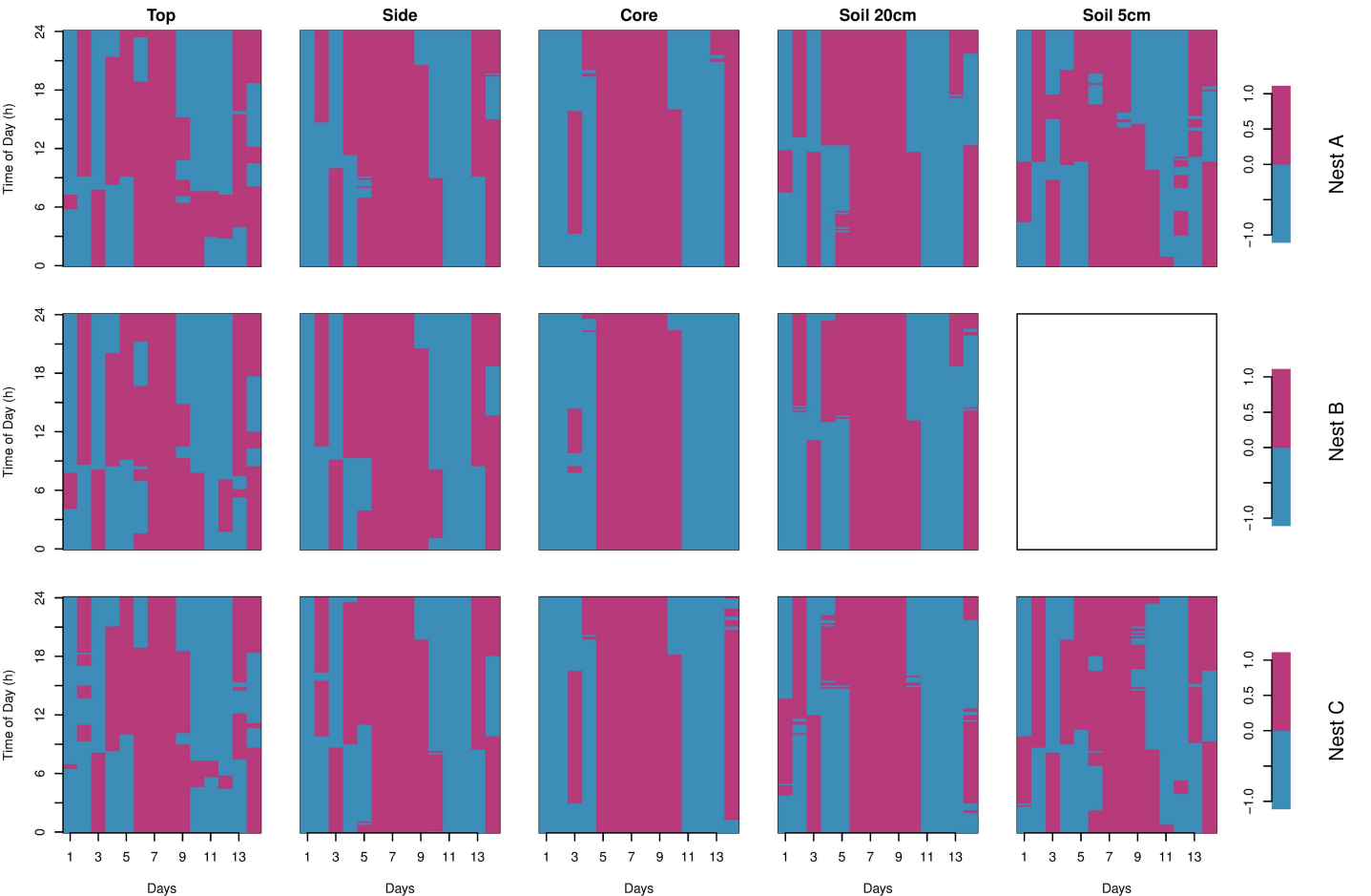


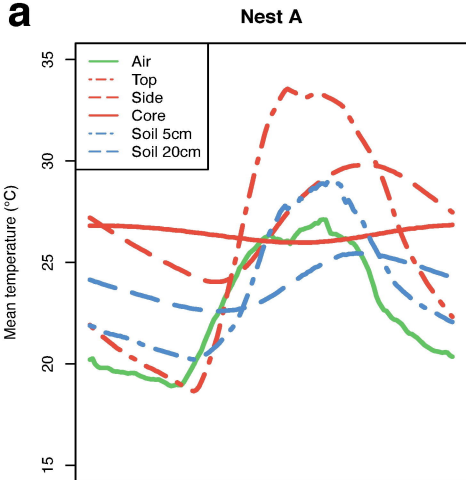
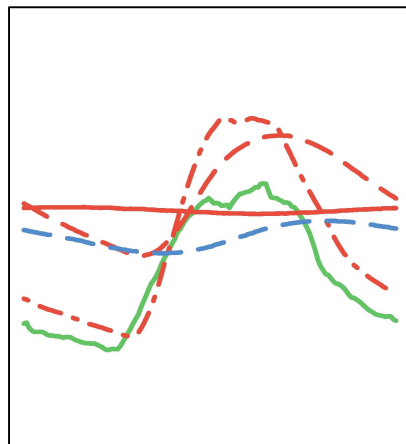
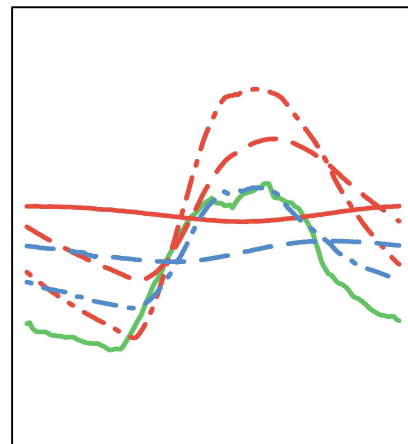
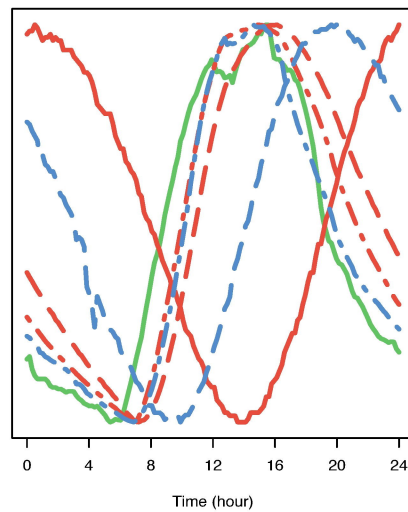
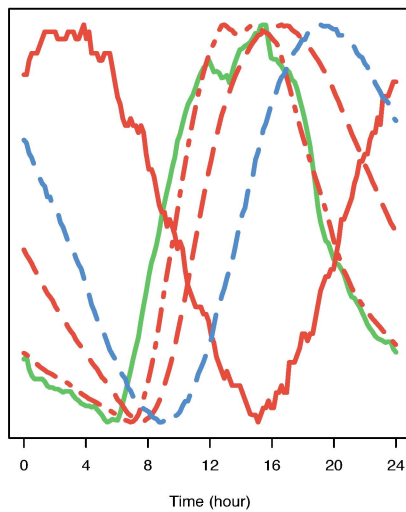
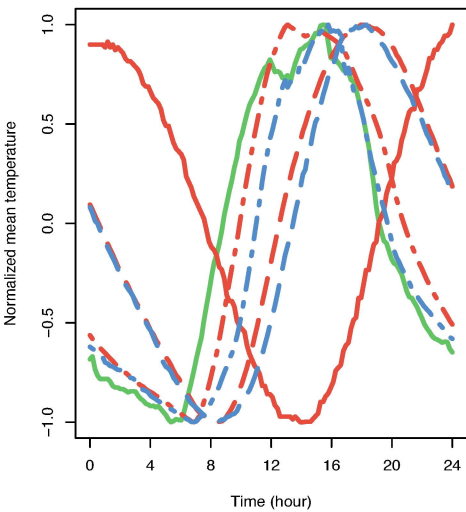


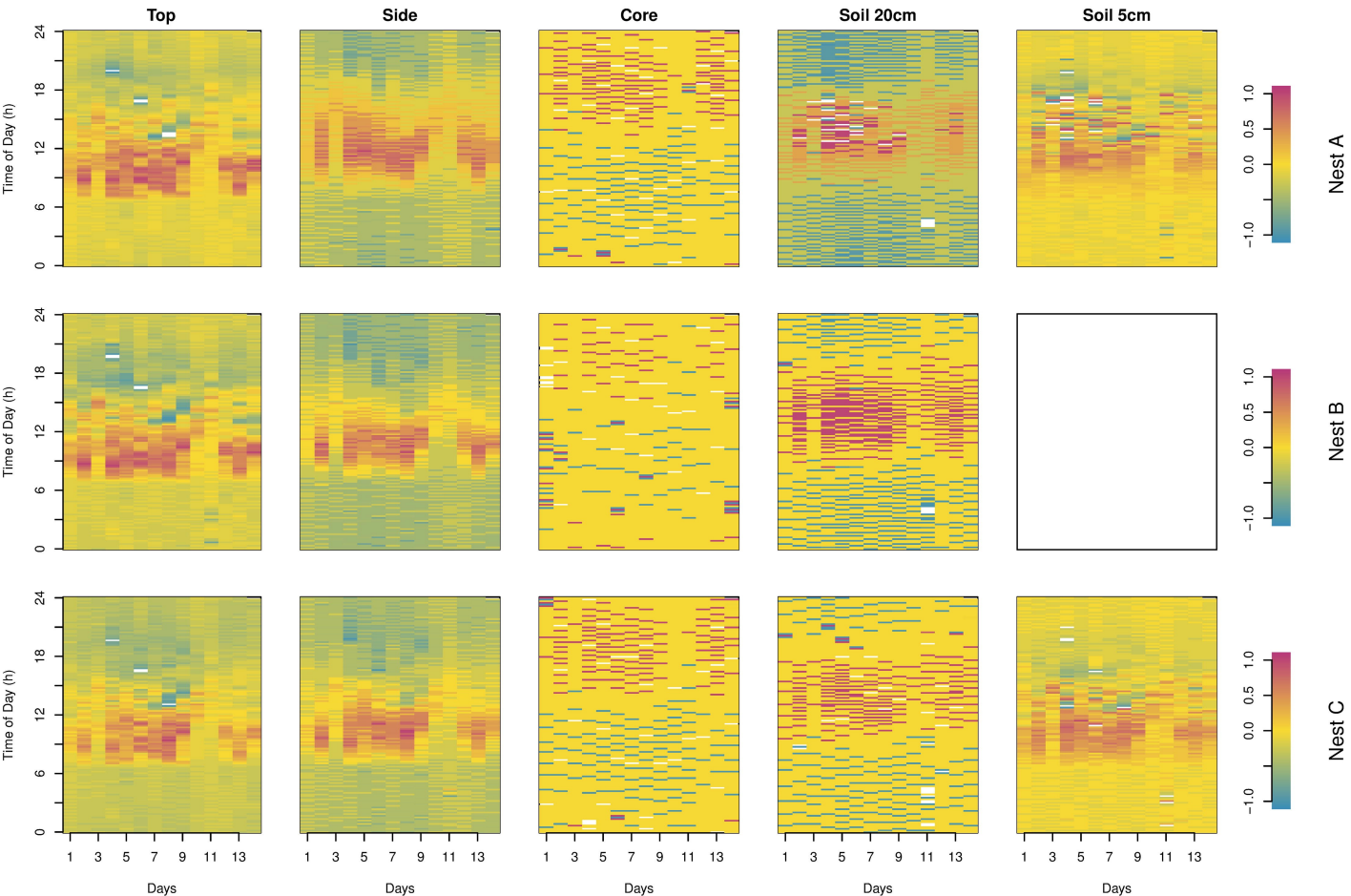


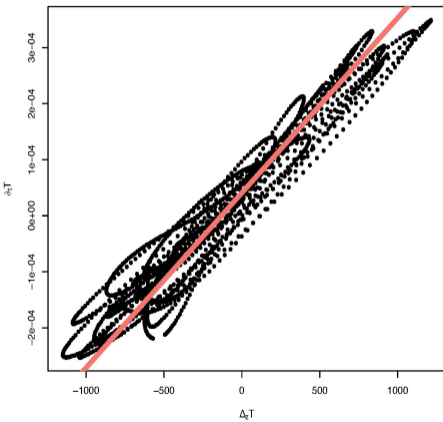
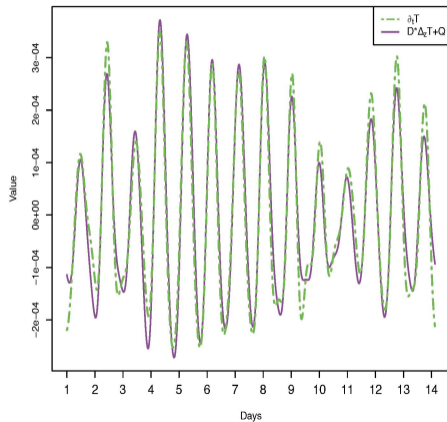
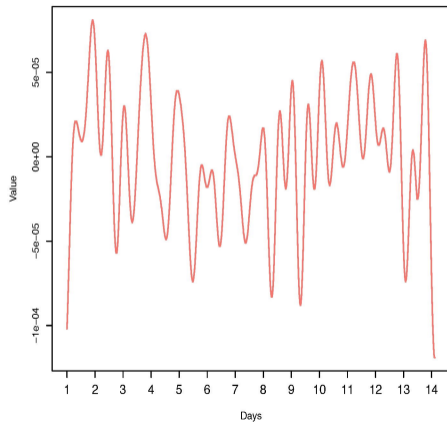


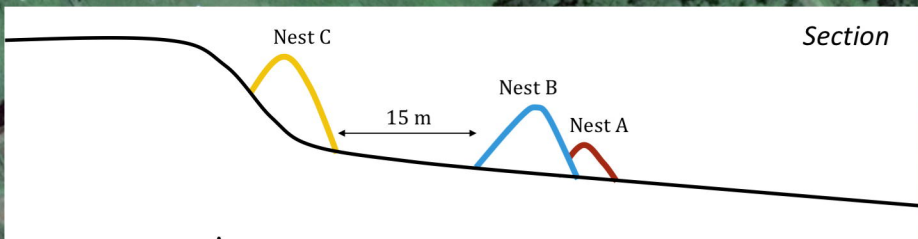








**a****Nest B****Nest C****b**

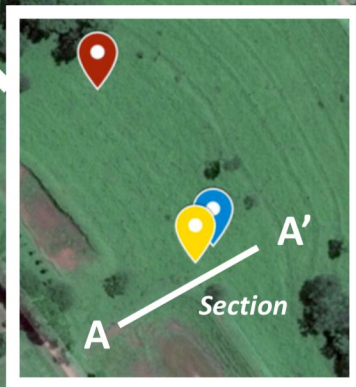



**a****b****c**



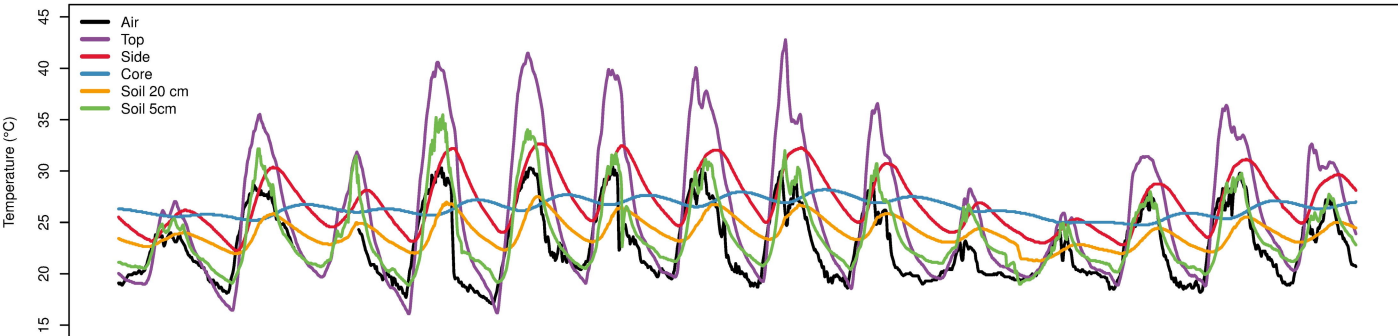
-  Nest A
-  Nest B
-  Nest C
-  Meteorological station

100 m

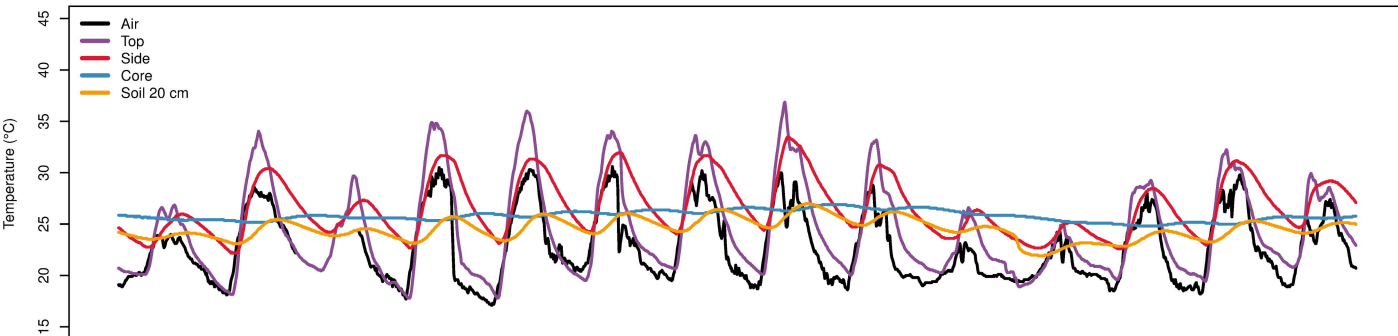




Nest A



Nest B



Nest C

